Results in Engineering 20 (2023) 101556

Contents lists available at ScienceDirect

Results in Engineering

journal homepage: www.sciencedirect.com/journal/results-in-engineering

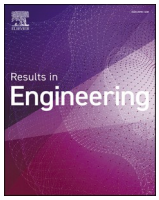

Monitoring and modelling the deformation of an aluminium prototype mould insert under different injection moulding and clamping conditions

Szabolcs Krizsma [a], András Suplicz [a,b,*]

[a] Department of Polymer Engineering, Faculty of Mechanical Engineering, Budapest University of Technology and Economics, Műegyetem rkp. 3., H-1111, Budapest, Hungary
[b] MTA-BME Lendület Lightweight Polymer Composites Research Group, Műegyetem rkp. 3., H-1111, Budapest, Hungary

ARTICLE INFO

Keywords:
Rapid tooling
Injection moulding
State monitoring
Injection moulding simulation
Coupled simulation

ABSTRACT

The conventional material of prototype injection moulds is aluminium. Well-established techniques are available on the applicability of such moulds, yet their operational state is not analysed comprehensively. State monitoring has huge benefits because the mould can be protected from excessive loads and deformations and product quality can be monitored in real time. In this paper, we measured the operational strains, cavity pressure and temperature distribution of prototype injection moulds with the traditional state monitoring method, and analysed the combined effect of holding pressure and clamping force on the operational deformations and cavity pressures. Increasing the clamping force and the holding pressure results in higher operational strains and cavity pressures. The precision of core shift analysis was tested if it can predict operational deformations of aluminium injection moulds. Core shift analysis could accurately predict the maximal deformation but it is inaccurate regarding the time when it occurs. A novel modelling method was also introduced where pressure and temperature results of the injection moulding simulation can be imported into finite element (FE) mechanical simulations. This way, mould deformations can be modelled in mechanical FE simulation environment. The measured operational deformations were compared both with core shift analysis results and with the coupled IM-FE simulation results. Core shift simulation can predict maximal deformations with adequate precision but it does not consider thermal expansion effects properly. In order to improve the accuracy of the simulations, a coupled IM-FE method is necessary, where excellent agreement can be found between the measurements and the calculations. The new, combined modelling technique can improve the accuracy of mould deformation modelling because additional mould material models become available in a professional finite element software. It can be especially useful in the modelling of polymeric mould inserts where stiffness is heavily temperature-dependent and the material creeps.

1. Introduction

Injection moulding is the most dynamically developing and diverse plastic processing technology. Innovative techniques like Rapid heat cycle moulding (RHCM) allows the fast variation of the mould surface temperatures at the different sections of the injection moulding cycle. Macedo et al [1] proved that the mechanical properties like the Young's modulus and the morphology (frozen layer thickness) of the injection moulded parts can be influenced by RHCM. Berges et al [2] and Naranjo et al [3] proved that special injection moulding techniques like Metal injection moulding (MIM) allows the production of functional metallic parts from thermoplastic polymer coated metal powder feedstock. The injection moulded parts are then debinded and sintered and the final metal part is obtained. It is clear that injection moulding is a versatile technology that has a large potential but also some significant limitations. Due to its large investment costs (both the injection moulding machine and mould making), it is typically profitable for large product volumes. On the other hand, product development time has to be reduced and the demand for more customizable parts is on the rise. These often contradictory needs can be served by Rapid Tooling (RT), which allows injection moulding trials before large-volume mould making. Rapid Tooling also makes flexibly customizable moulds

* Corresponding author. Department of Polymer Engineering, Faculty of Mechanical Engineering, Budapest University of Technology and Economics, Műegyetem rkp. 3., H-1111, Budapest, Hungary.
E-mail address: suplicz@pt.bme.hu (A. Suplicz).

https://doi.org/10.1016/j.rineng.2023.101556
Received 14 July 2023; Received in revised form 4 October 2023; Accepted 30 October 2023
Available online 2 November 2023

feasible. Several case studies are available on metallic RT inserts manufactured by Direct Metal Laser Sintering (DMLS). Kuo et al. [4] analysed different conformal cooling channel layouts to enhance the cooling efficiency of DMLS printed injection moulds. Park et al. [5] produced an injection mould by Laser Powder Bed Fusion (LPBF) containing lattice structures, and successfully reduced the weight of the mould while maintaining sufficient stiffness and longevity. Park et al [6] applied Selective Laser Melting (SLM) to produce an injection mould insert with conformal cooling channels. This way, the cooling efficiency of the injection mould was increased. Török et al [7] also applied LPBF to print a steel shell (incorporating conformal cooling channels) that they later cast with copper to create an injection mould with excellent heat extracting capability. Lupone et al. [8] analysed the optimal processing parameter window for Selective Laser Sintering (SLS) based on the mechanical properties, dimensional accuracy, and defect content of the sintered parts. Alkentar et al. [9] analysed the dimensional accuracy of lattice structures printed by DMLS. They concluded that as the size and geometric complexity of the printed parts grew, the dimensional accuracy of the parts decreased. Mahshid et al [10] also proved that SLM makes new, complex geometries feasible, such as lattice structures and that the strength and stiffness of these structures are comparable with their solid counterparts. Narvan et al [11] analysed the deflections and residual stresses of the part after LPBF printing and offered solutions for minimizing them. Metal printing is a promising direction in injection mould making but it still has problems that need to be solved, such as part warpage and residual stresses.

Low-volume injection moulds are easy to manufacture by polymeric additive technologies like Material Jetting (PolyJet), Vat photopolymerisation (stereolitography) or Selective Laser Sintering (SLS). Zink et al [12] proved that injection mould inserts printed by PolyJet can be successfully applied to injection mould polymeric parts in low-volume. Freeform geometries like conformal cooling are also feasible that enhance cooling efficiency and reduce cycle time. Mendible et al [13] had similar finding in their comparative study of PolyJet printed, DMLS printed and conventional machined injection mould inserts. Ilyas et al [14] demonstrated the applicability of SLS-printed injection mould inserts in their comprehensive case study. Davoudinejad et al [15] analysed the effect of thermal aging on the lifetime of vat photopolymerisation printed injection mould inserts and found the technology suitable to print low-volume injection moulds. Additively manufactured polymeric moulds can make injection moulding more flexible but the reachable cycle numbers are relatively low and careful choice of processing parameters is essential. Due to these, conventional machined aluminium mould inserts are here to stay for a long time as the leading prototype injection mould making technique.

Besides the appearance of additive technologies, another potential direction of development is the comprehensive sensoring and metrology of injection moulds. It is uncommon in the current industrial environment even though it is clearly beneficial for real-time product quality monitoring and mould life expectancy. Ageyeva et al [16] summarised the wide array of different sensors that are available, including temperature and pressure sensors. Advanced machine learning algorithms can characterize product quality based on for example, the measured cavity pressure curves. Párizs et al. [17] successfully applied four different machine-learning algorithms (k nearest neighbour, naïve Bayes, linear discriminant analysis, and decision tree) to determine the quality of injection moulded products based on the measured cavity pressure curves. Struchtrup et al. [18] applied different mathematical models to predict product thickness and mass based on the measured cavity pressure curves using different injection moulding parameter sets. Ke et al. [19] used a multilayer perceptron (MLP) neural network and quality indices based on holding pressure, peak pressure, residual pressure drop and the pressure integral to effectively classify the parts as "qualified, unqualified and to be confirmed". Pressure integral is an effective tool to monitor product quality in real time. Vukovic et al. [20] applied process controlling mathematical models to effectively control cavity pressure throughout the injection moulding cycle. Zhou et al. [21] proved that the pressure integral shows strong correlation with product mass and it is more stable and consistent than only the peak pressure value. Wang et al. [22] also concluded that the correlation between the cavity pressure integral and the product mass is stronger than the correlation between the peak pressure and the product mass. Kurt et al. [23] also applied piezoelectric pressure sensors and analysed correlations between the cavity pressure curves and product dimensions. They concluded that cavity pressure curves and mould temperature shows a strong correlation with part shrinkage. Tsai et al. [24] applied an artificial neural network (ANN) and response surface methodology (RSM) to set the optimal processing window of cooling time and packing time for injection moulding lenses. They found ANN to be better and more accurate for setting up the processing window. Chen et al. [25] suggest the strain measurement of the injection moulding machine tie bar as a quality monitoring tool. Su et al. [26] suggest the combination of the strain measurement of the injection moulding machine tie bar with nozzle pressure measurement. The combination of the two can be effective in product quality monitoring. Krizsma et al. [27] proved that the concept of comprehensive state monitoring of injection moulds (including simultaneous strain, cavity pressure and temperature measurement) is new and it has a high research potential. Krizsma et al. [28] also proved that comprehensive state monitoring could greatly help to adjust the injection moulding processing parameters that can improve the longevity of prototype mould inserts.

Injection mould deformations have a profound effect on the product quality and the longevity of the moulds. Operational deformations of injection moulds are hard to measure but researchers have already created different methodologies to solve that. Mahshid et al [29] placed inductance probes on a multi-cavity injection mould and measured the operational displacements. They were able to measure deformations with an accuracy of approximately 10 μm. Zhao et al [30] applied an ultrasonic method to measure the stress in an injection moulding machine tie-bar. The proposed measurement method can estimate the clamping force during operation. Huang et al [31] measured the elongation of the injection moulding machine tie bar to calculate the clamping force. They created an algorithm to set the proper clamping force based on the measured elongations. Jung et al [32] created a mathematical model that calculates the mould deformation as a combination of melt pressure induced deformation and heat induced thermal expansion. Several measurement and modelling methods were already elaborated to quantify the operational state of injection moulds, however they were not integrated into a comprehensive monitoring system that measures all the important process parameters simultaneously. Analysis of correlations between the measured process parameters and the resulting product properties is also rare to find. The simulation of the operational deformation of injection moulds is also a scarcely researched topic. These are the main knowledge gaps that this study aims to fill.

This research presents a novel measurement system that simultaneously monitors the pressures, operational strains and the thermal state of an injection mould insert. The measured cavity pressure data was used in monitoring product quality with excellent correlations. Cavity pressure measurement is already widely applied and popular in injection moulding. Excellent correlations between the measured cavity pressure and product properties prove its suitability for real-time product quality monitoring. We also introduced two simulation methods (core shift simulation in Autodesk Moldflow Insight and coupled injection moulding simulation and finite element mechanical simulation in ANSYS Workbench Mechanical) to calculate the operational deformations of the mould inserts. The results of both simulation methods were validated with the measured operational strains, cavity pressures and temperature distributions and there was a satisfactory agreement between them. The coupled injection moulding and finite element mechanical simulation can compensate for some shortcomings of core shift analysis. A significant simplification of core shift analysis is that only a

constant parameter, linear elastic material model is available for the injection mould inserts. Professional finite element mechanical simulation can also incorporate viscoelastic material models. These material models can also model the increasingly popular and widely used polymeric moulds and mould inserts more accurately in the future.

2. Materials and methods

2.1. Injection moulding parameters

An Arburg Allrounder 270S 400-170 injection moulding machine (with the screw diameter of 30 mm) was used for the injection moulding series. The injection moulded material was a polypropylene homopolymer (Tipplen H145F, MOL Group PLC). It is ideal because of its excellent Melt Flow Rate (29 g/(10 min) at 230 °C and 2.16 kg). Table 1 shows the injection moulding parameters used.

2.2. The test mould

A two cavity steel mould housing was applied and only the upper cavity was used for the injection mouldings. The product was a plate that had the dimensions of 65 mm × 55 mm x 2 mm. The cavity was filled through an edge gate. Fig. 1 shows the test mould with the location of the sensors.

Strains were measured with two gauges (KMT-LIAS-06-3-350-5EL) and a Spider8 unit (Hottinger Baldwin Messtechnik GmbH) collected the data. Cavity pressure was measured with an RJG Piezo 6159 piezoelectric pressure sensor and its data was collected with a Kistler CoMo unit. Temperature was measured with a Heraeus M222 Pt100 thermocouple and an Ahlborn Almemo 8990–6 unit collected its data. The cavity inserts in both mould halves and the two spacer inserts underneath them were machined from EN AW 5754 O/H111 aluminium alloy. Table 2 contains its relevant mechanical and thermal properties. The material has acceptable strength and stiffness and it shows excellent thermal conductivity compared to conventional steel moulds.

3. Results and discussion

3.1. Injection moulding series at constant parameters

The first part of the injection moulding series was the finding of complete volumetric filling. In this segment of the injection moulding series, no holding pressure was applied. After finding the proper switchover point, we injection moulded 10 cycles at a constant holding pressure of 75 bar. This phase characterizes the stability and reproducibility of the technology. These 10 cycles were injection moulded at all four analysed clamping forces (5, 10, 15 and 20 t). No residual deformations occurred after the cycles due to the relatively low mechanical load, therefore the reproducibility of the cycles was satisfactory. Fig. 2 presents the near-gate strain curves in the case of the 5 t clamping force.

The increase in clamping force results both in a greater strain

Table 1
Injection moulding parameters.

Parameter	Value
Melt temperature (°C)	190
Injection speed (cm^3/s)	15
Injection pressure limit (bar)	500
Dose volume (cm^3)	40
Switchover point (cm^3)	25.5
Holding pressure (bar)	50 to 300
Clamping force (t)	5 to 20
Holding time (s)	15
Residual cooling time (s)	30
Idle time (s)	250

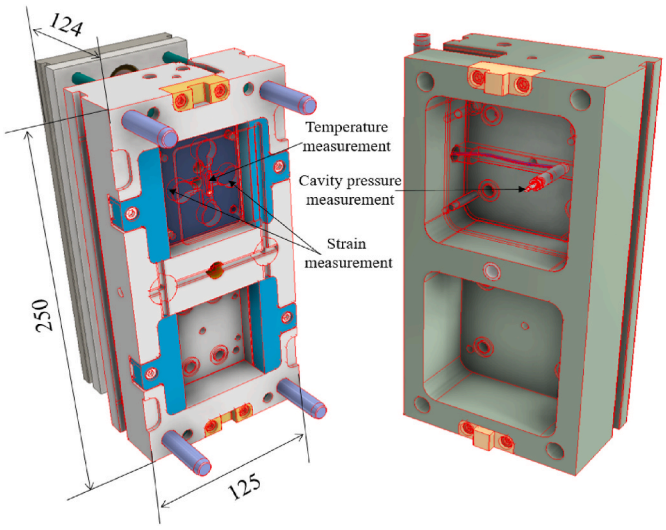

Fig. 1. The test mould.

Table 2
Mechanical and thermal properties of EN AW 5754 O/H111.

Parameter	Value
Tensile strength (MPa)	160–200
Elongation at break (%)	12
Modulus of elasticity (GPa)	68
Thermal conductivity (W/(m·K))	147
Coefficient of thermal expansion (1/K)	$24 \cdot 10^{-6}$

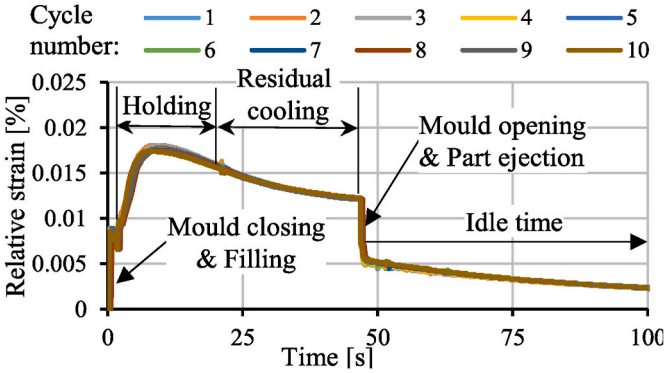

Fig. 2. Relative strain curves (near the gate) at a constant holding pressure of 75 bar and with a clamping force of 5 t.

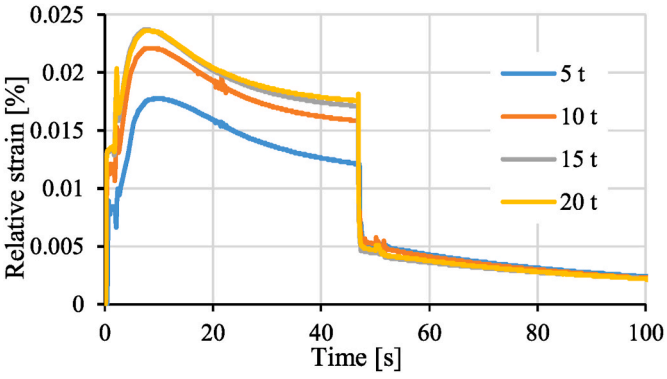

Fig. 3. Relative strain curves (near the gate) at a constant holding pressure of 75 bar and with increasing clamping force.

increase at mould closing and in a steeper decrease at mould opening. Fig. 3 presents the relative strain curves at the same cycle at the four different clamping forces. It can be seen that at a clamping force of 5 t, the maximal relative strain is 0.018 %, which increases to 0.022 % at clamping forces of 10 t and 15 t. The maximal relative strain at a clamping force of 20 t is 0.024 %. At this low holding pressure (75 bar), where mould opening does not occur, the increase in clamping force adds an offset to the operational strains. There is no significant difference in the relative strain between the 15 t and 20 t clamping force levels. A suitable clamping force is needed to prevent mould opening but in the meantime subject the insert to the lowest mechanical load possible.

Fig. 4 shows the cavity pressures for the constant holding pressure section at a clamping force of 10 t. The cavity pressure curves are almost identical in each cycle, which also proves the excellent reproducibility of the technology. This kind of repeatability was observed with all clamping forces.

The first spikes in the cavity pressure–time curves correspond to complete volumetric filling, where the melt reaches the end of the flow length. After that, the downturn is caused by the pressure loss occurring at the switchover from filling to holding. Maximal injection pressure was above 300 bar at switchover, which decreased to the pre-set 75 bar in the holding phase. The second pressure increase is caused by the additional material injected into the cavity to compensate for product shrinkage. The second spike is likely ended by gate freeze where holding pressure on the product cannot be maintained longer. From gate freeze until part ejection, the cavity pressure remained constant as the frozen part pressed the head of the direct piezoelectric pressure sensor. The second spike in the cavity pressure was eliminated at higher holding pressures, because the injection pressure loss at switchover was significantly lower.

Fig. 5 presents the effect of increasing clamping force on the measured cavity pressure curves. The applied clamping force heavily influences the first spikes, corresponding to volumetric filling and the switchover. Maximal cavity pressure at the end of filling was 26 bar at 5 t, 40 bar at 10 t, 67 bar at 15 t and 69 bar at 20 t. As higher clamping forces were applied, the injected melt could not increase its available space in the cavity (and most likely cavity volume was lower due to increasing mould deformations), which resulted in higher cavity pressure. Further segments of the cavity pressure curves (corresponding to holding, residual cooling and mould opening) do not depend on the applied clamping force.

3.2. Injection moulding series at increasing holding pressures

After injection moulding at constant parameters, we increased holding pressure from 50 bar in every second cycle in 25 bar steps. Holding pressure was increased in all four injection moulding series, corresponding to the four analysed clamping force levels. Holding pressure was increased to 300 bar because at this point the mould

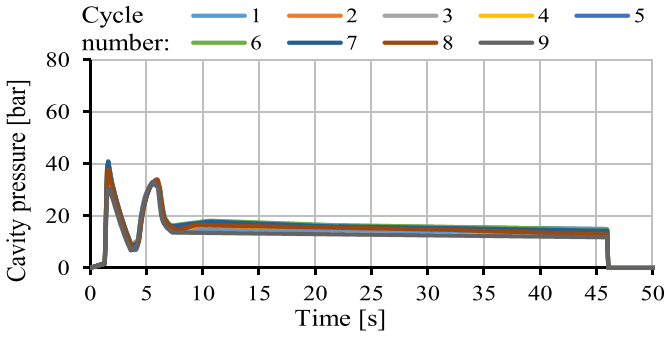

Fig. 4. Cavity pressure curves at a constant holding pressure of 75 bar and with a clamping force of 10 t.

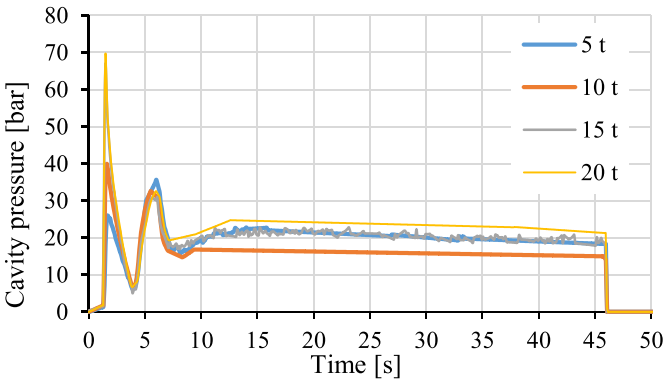

Fig. 5. Cavity pressure curves at a constant holding pressure of 75 bar, with increasing clamping force.

opened at the lowest, 5 t clamping force. Fig. 6 shows the combined effect of holding pressure and clamping force on the resulting operational strains.

With lower clamping forces, the relative strain curves show higher scatter with increasing holding pressure. As holding pressure increases, so does the overall injected melt volume that gradually opens the mould along the parting plane. With a clamping force of 5 t and a holding pressure of 275 bar, the opening of the mould is clearly indicated by the sawtooth-shaped sections of the corresponding relative strain curve. Abrupt changes in the relative strain curves can indicate partial mould opening and flash. This unwanted mould opening can be compensated for with higher clamping forces, and the relative strain curves become less divergent.

Fig. 7 shows the cavity pressure curves at the different holding pressures and clamping forces. Cavity pressure maximums were increased both by the higher holding pressure and the increasing clamping force. The first maximums corresponding to volumetric filling decayed more slowly around the switchover point and stabilized at higher values in the holding and residual cooling phases.

3.3. Product quality analysis

Clamping force also has a profound effect on product quality. Fig. 8 shows product mass at different holding pressures and clamping forces. In the constant holding pressure section, product masses remained constant with each clamping force. Increasing the clamping force resulted in slightly lower product masses, since the available cavity volume decreased as the mould was more compressed. As holding pressure increased, so did product mass, and the effect of insufficient clamping and gradual mould opening is clearly indicated in the curve of the 5 t clamping force. The tendency remained that higher clamping force results in smaller product mass at the same holding pressure. Product mass measurement can be an easy and effective tool in determining adequate clamping force.

Another promising product quality control tool is the monitoring of the cavity pressure integral. It was calculated as the area under the cavity pressure–time curve from the start of the holding phase to the end of the holding phase, because that is the time when additional material is injected into the cavity and shrinkage compensation occurs. We assumed a linear correlation between the calculated pressure integrals and the measured product masses, and found satisfactory correlations (mostly $R^2 > 0.9$) at the analysed clamping forces. The linear correlation can be expressed mathematically as follows:

$$m_{prod} = c_1 \cdot \int_{t=start\ of\ holding}^{t=end\ of\ holding} p_{cavity}(t)\mathrm{d}t + m_0 \quad (1)$$

In Eq. (1), the c_1 parameter characterizes the proportionality between product mass and the pressure integral. It is primarily determined

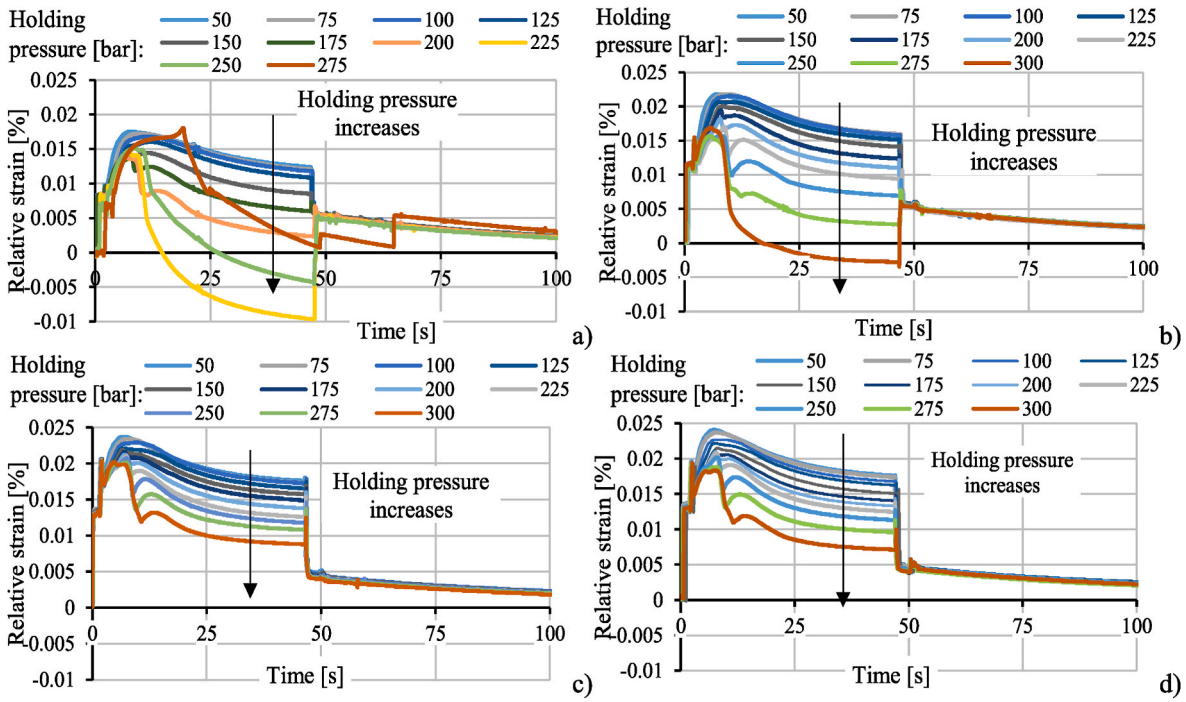

Fig. 6. Relative strain curves at increasing holding pressures with a clamping force of 5, 10, 15 and 20 t (a, b, c and d, respectively).

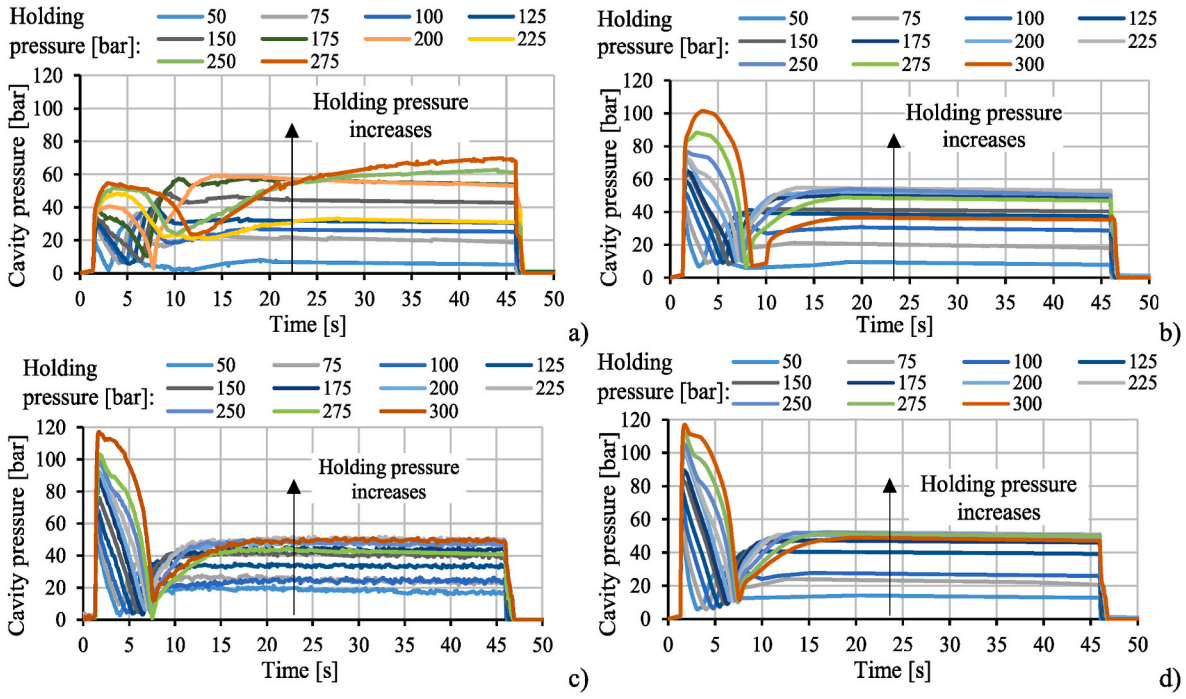

Fig. 7. Cavity pressure curves at increasing holding pressures with a clamping force of 5, 10, 15 and 20 t. (a, b, c and d respectively).

by mould stiffness (mould material and local geometry) and is also influenced by the loading condition (clamping force in this case). The m_0 parameter is the static product mass, which can be measured at zero cavity pressure, meaning zero shrinkage compensation by holding pressure. The m_0 parameter also depends on the clamping force, since the compression of the mould insert influences the available cavity volume. Gradual mould opening occurred at the lowest, 5 t clamping force, as was already proved by product mass (Fig. 8). Therefore, the last few cycles (indicated by the grey hollow circles in Fig. 9) had to be excluded from linear fitting. This also highlights that proper clamping is a prerequisite for the strain integral to function as an ideal product quality monitoring tool. If flash can be prevented, the pressure integral can be used with acceptable confidence to identify scrap and product mass deviations.

Formally, similar correlations can be found between product thicknesses (both near the gate and far from the gate) and the measured pressure integrals. Fig. 10 shows these results. If an adequate clamping force is applied (in this case 10 t or more), the pressure integral can

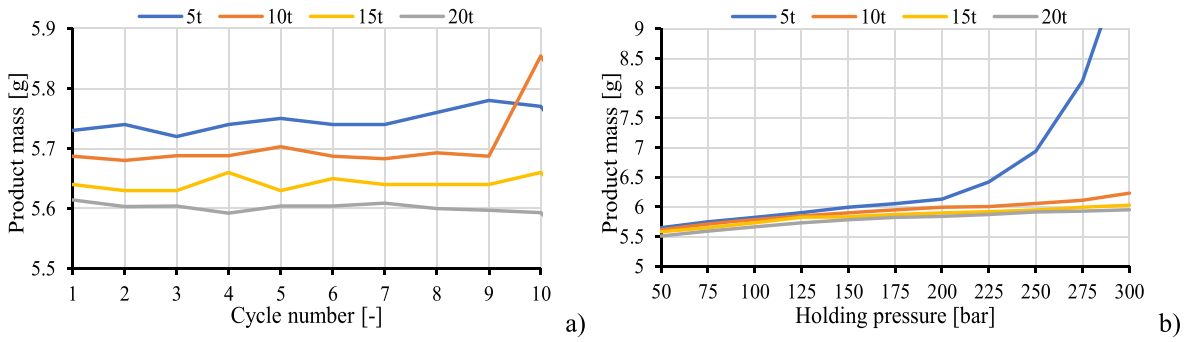

Fig. 8. Product masses at different clamping forces at a constant holding pressure of 75 bar a) and increasing holding pressure b).

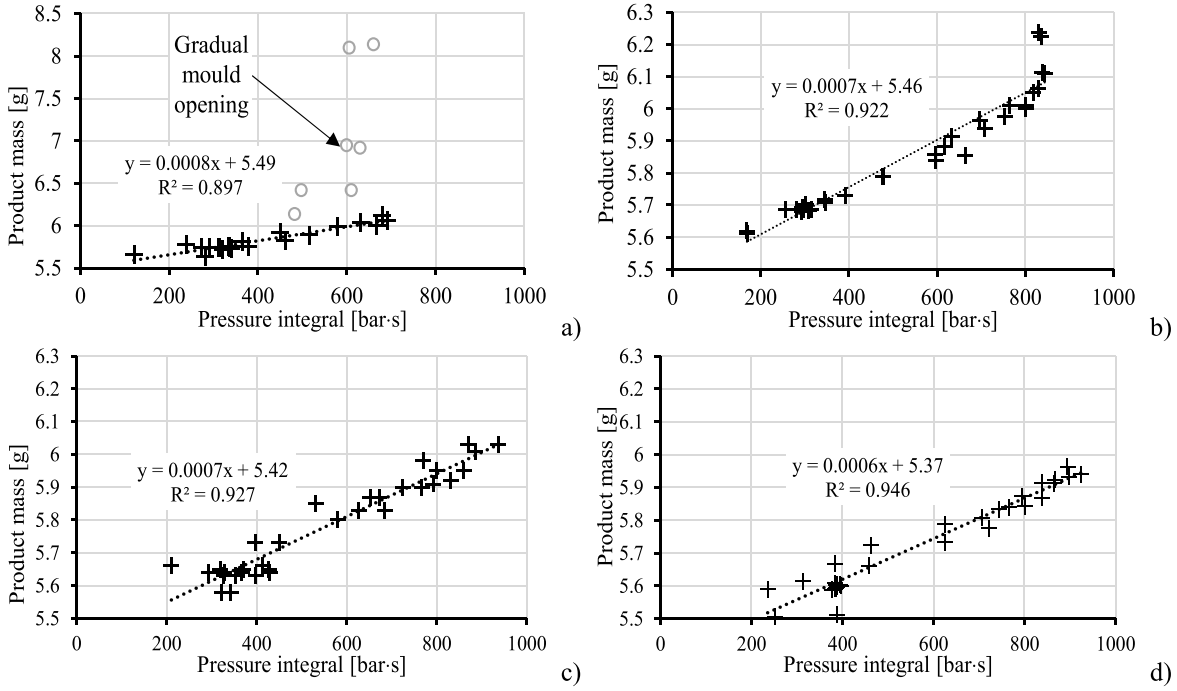

Fig. 9. Correlational diagrams between the pressure integral and product mass at a clamping force of 5 t, 10 t, 15 t, and 20 t. (a, b, c and d, respectively).

predict product thickness with satisfactory confidence (mostly $R^2 > 0.9$). The correlation between product thickness and the pressure integral can be expressed with Eq. (2), where c_2 is the proportionality factor between the pressure integral and product thickness. The c_2 factor is also determined by the material and the local geometry of the mould. W_0 is static product thickness, which can be measured at zero shrinkage compensation by holding pressure.

$$w_{prod} = c_2 \cdot \int_{t=start\ of\ holding}^{t=end\ of\ holding} p_{cavity}(t)\mathrm{d}t + w_0 \tag{2}$$

Fig. 10 shows the analysis of correlation between the pressure integral and product thickness.

Table 3 shows the parameters of linear fitting. Higher clamping forces resulted in lower static product masses (m_0) and lower proportionality factors between the pressure integral and product mass (c_1). The decrease in both parameters indicates that the same pressure integral results in lower product mass at greater clamping forces. It is as expected because a higher clamping force compresses the mould more and reduces the available cavity volume. Static product thickness (w_0) also decreased steadily near the gate as clamping force increased. However, far from the gate, static thickness remained relatively stable without a decreasing tendency. Product thickness variation is especially sensitive to the imperfect contact between the moving and the stationery side mould inserts, which is a result of manufacturing tolerances.

3.4. Thermal results

The thermocouple (Fig. 1) measured the temperature at the back of the insert during the injection moulding series. Fig. 11 shows the measured temperatures.

The curve clearly indicates an overall increasing tendency. Insert temperature at the back grew from the ambient temperature (~28 °C) to ~41 °C by the start of the last cycle. The insert heats up fast, due to the outstanding thermal conductivity of the aluminium insert material. We assumed that the stiffness of the insert material is practically constant in the operational temperature range.

4. Simulation of the insert's operational state

After the injection moulding series, we performed an injection moulding simulation in Autodesk Moldflow Insight 2021 to reproduce the measured results. The Core Shift module of the software was used to calculate the operational deformation of the insert. We also created an additional simulation model, where we calculated the operational

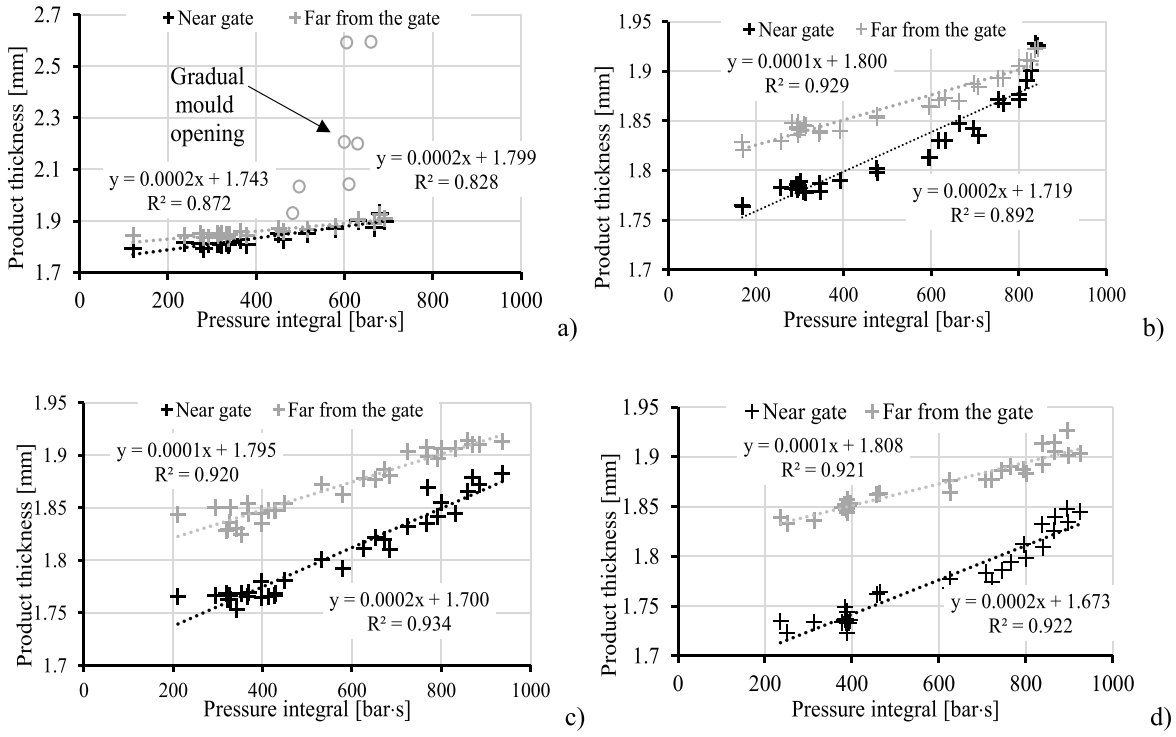

Fig. 10. Correlational diagrams between the pressure integral and product thickness with clamping forces of 5 t, 10 t, 15 t and 20 t. (a, b, c and d, respectively).

Table 3
Parameters of the linear correlations between the cavity pressure integral and product properties (mass and thickness).

Clamping force [t]	c_1 $[\frac{g}{bar \bullet s}]$	m_0 [g]	c_2 $[\frac{mm}{bar \bullet s}]$	w_0 [mm]
5	0.0008	5.49	0.0002/0.0002	1.743/1.799
10	0.0007	5.46	0.0002/0.0001	1.719/1.800
15	0.0007	5.42	0.0002/0.0001	1.700/1.795
20	0.0006	5.37	0.0002/0.0001	1.673/1.808

temperature and pressure distribution of the cavity surface (using IM simulation), and exported the nodal pressure and temperature results to the ANSYS Workbench Mechanical 2019 finite element simulation software using the "mpi2ans" macro in Moldflow Insight. We created the mechanical model in ANSYS as well and compared the calculated deformation to the measured deformation and the core shift simulation results. The workflow is explained in Fig. 12.

4.1. Moldflow simulation

We modelled strain gauges by splitting the slot surfaces (Fig. 13). Strain was calculated from the Y directional nodal displacements of the characteristic points of the gauge (numbered 1 to 6).

The applied strain gauges can measure strains in the Y direction (in the coordinate system of Fig. 13). Strain was calculated as the difference of the average nodal displacements at the two ends of the strain gauge divided by the unloaded length of the conductor of the gauge (L_0). It can be expressed mathematically with Eq. (3)-(4).

$$\overline{U_{y,A}} = \frac{U_{y,1} + U_{y,2} + U_{y,3}}{3}; \overline{U_{y,B}} = \frac{U_{y,4} + U_{y,5} + U_{y,6}}{3} \quad (3)$$

$$\overline{\varepsilon_{y,AB}} = \frac{\overline{U_{y,A}} - \overline{U_{y,B}}}{L_0} \quad (4)$$

Fig. 14 shows the calculation model for core shift simulation. The applied analysis sequence was Fill + Pack. The contacting surfaces of the mould were modelled with the use of the "One-sided constraint". It prohibits deformation towards the mould housing wall, but the insert can detach from the wall. Sufficient mesh density (4-node tetrahedral

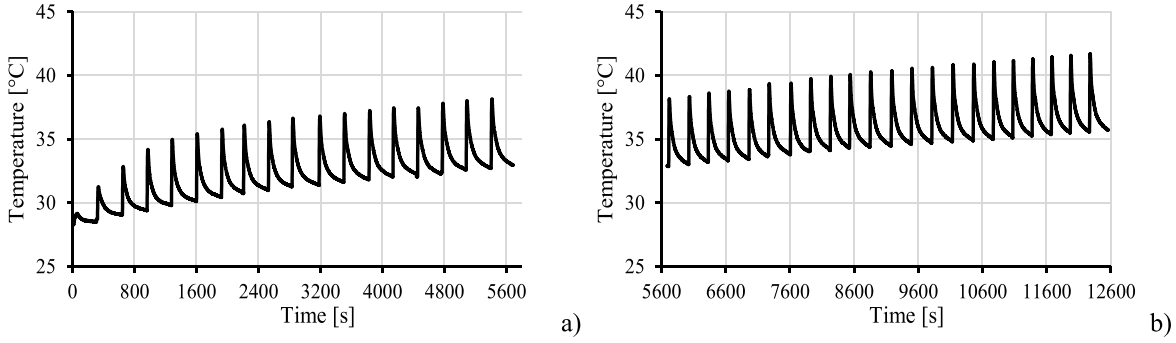

Fig. 11. Temperature measured by the thermocouple (15 t clamping force). Holding pressure was a constant 75 bar a) and increasing b).

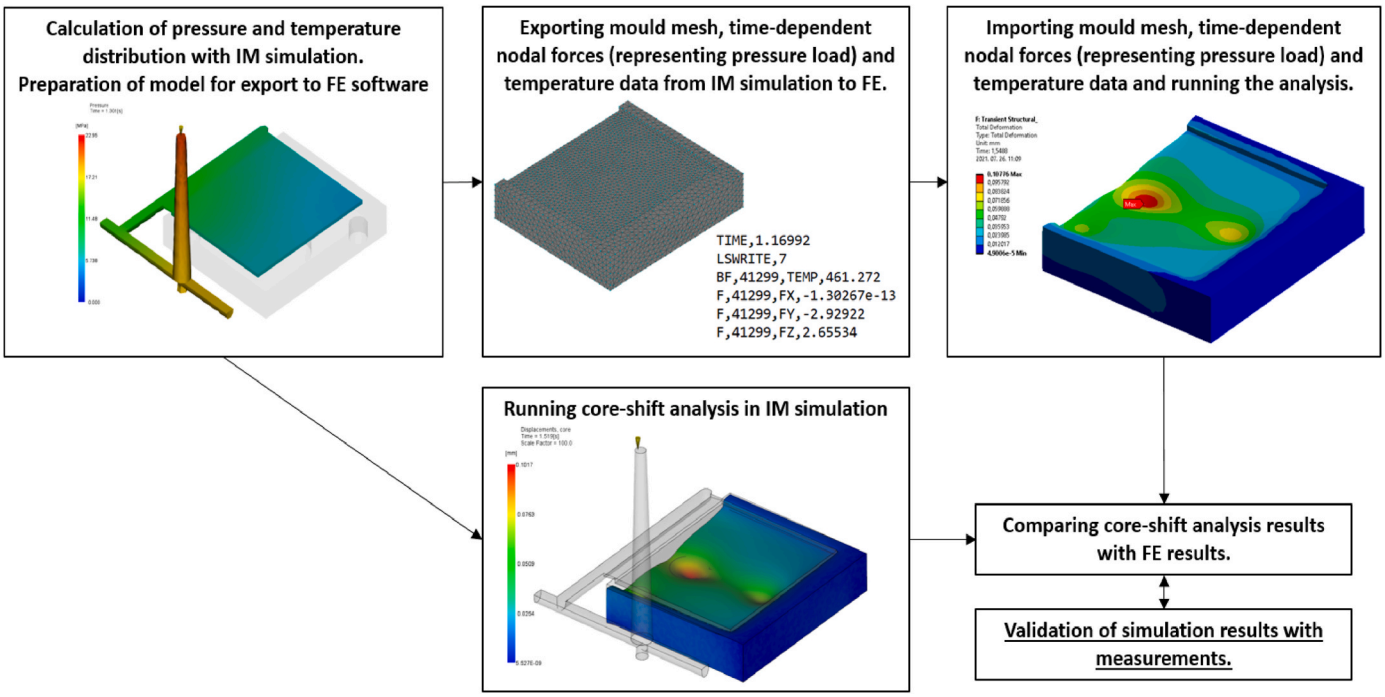

Fig. 12. The workflow of the simulation.

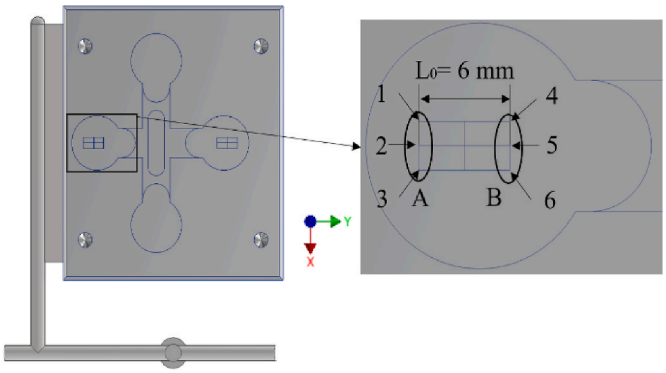

Fig. 13. The simulation of the strain gauges.

elements for the product and the mould insert) was applied on the cavity surface–product contact region, around the edge gate as well as at the slots of the strain gauges and the thermocouple. The product mesh consisted of 69 393 nodes and 377 928 elements, while the mould insert mesh consisted of 61 914 nodes and 344 426 elements. Global edge length was 3 mm and additional refinements were applied to the cavity–product contact surfaces and the gate area (with an edge length of 1 mm). Core shift analysis was performed with a maximal volume filled increment of 5 % and a maximum time step of 0.1 s between two analyses. Insert temperature was calculated as a "transient during flow for all part inserts and cores". Core shift analysis was performed for filling, packing and residual cooling as well. The mesh was automatically updated during the core shift analysis.

One of the most crucial parameters of injection moulding simulation is the heat transfer coefficients (HTC) between the melt and the cavity walls. Heat transfer coefficients primarily depend on the pressure of the melt against the cavity wall and the temperature difference between the polymer and the cavity wall. The cavity pressure is influenced by both the holding pressure and the clamping force (if the injected volume is unchanged), as it was presented by Fig. 7. Heat transfer modelling is crucial, yet only a few studies focus on it [33]. Moldflow performs core deformation calculations only until the melt freezes. After that, it

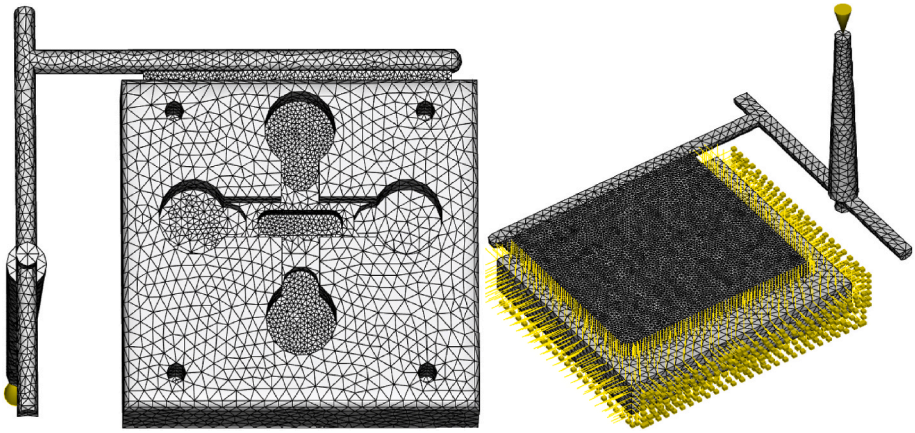

Fig. 14. The core shift simulation model. (The yellow sticks indicate the One-sided constraints on the mould mesh nodes.)

assumes the nodal displacements of the mould insert constant [34]. Therefore, the core shift analysis algorithm does not fully take into account the springback of the cooling product and thermal expansion. Moldflow models heat transfer in three sections: filling, packing and residual cooling and it sets different heat transfer coefficients for each. Due to the relatively low pressures, heat transfer coefficients were assumed to be lower than the default. We made a parameter sensitivity study, where the default HTC values in Moldflow, half the values and one fifth of the values were analysed. Table 4 shows these heat transfer coefficients.

The adequacy of the heat transfer coefficients was determined based on the measured insert temperature data (acquired by the thermocouple at the back of the insert). Results were saved in 10 time steps (both in the filling and the holding phases) and in 5 time steps in the residual cooling phase. The analysed holding pressure in the simulations was 75 bar, because we did the 10-cycle repeatability test at that pressure. The results of the Moldflow simulation were validated with the measured results at 5 t clamping force.

We compared the modelled thermal state of the insert at the location of the thermocouple to the actual measured temperature (Fig. 15). The most accurate temperature–time curve was reached with the 1/5 HTC model; the maximal difference in the measured and the simulated temperature is 3 °C. Measured temperature curves can be ideal tools for setting the proper heat transfer coefficients in future simulations. Based on the comparison of the measured and the simulated temperature distributions, we found the 1/5 HTC model to be the most accurate, therefore we only evaluated product dimensional accuracy and the simulated strain results with this heat transfer coefficient.

Another way to prove the accuracy of the simulation is to compare the measured and calculated product thicknesses. In Moldflow, we used volumetric shrinkage (s_{vol}) to calculate product thickness (w_{calc}) from nominal product thickness (w_{nom}). The calculated thicknesses were compared to the actual measured thicknesses in seven points overall. Product thickness was calculated with Eq. (6):

$$w_{calc} = \frac{100 - s_{vol}}{100} \bullet w_{nom} \tag{6}$$

We found a satisfactory match between the measured and the calculated thicknesses (Fig. 16).

Table 5 shows the calculated and the average measured product thicknesses. In the 1/5 HTC model, the maximal difference between the simulation and the measured thickness was only −5.40 % out of seven analysed locations, covering the injection moulded product almost entirely. These results indicate that product dimensions can be calculated with good accuracy, if heat transfer is modelled properly. Also, when core shift analysis is used, the finite rigidity of the cavity can also be considered. It is especially helpful when there are thin, low-rigidity cavity inserts that tend to deform under operational pressure load.

Fig. 17 shows the calculated total deformation field with the use of core shift simulation. The deformation field is in line with preliminary expectations. The deformations are mainly concentrated in the region of the strain gauge slots since local wall thickness and stiffness is lower there. The slot near the gate is subjected to higher deformations than the slot far from the gate, which can be explained by the pressure drop along the flow length.

We compared the average strains, calculated according to Fig. 13 and Eq. (3) and (4), to the measured strains and found adequate matching between the maximal strains obtained by core shift analysis and actual measurements (Fig. 18).

Table 4
The analysed heat transfer coefficients.

IM cycle element	Default HTC [W/(m²K)]	1/2 HTC [W/(m²K)]	1/5 HTC [W/(m²K)]
Filling	5000	2500	1000
Packing	2500	1250	500
Residual cooling	1250	625	250

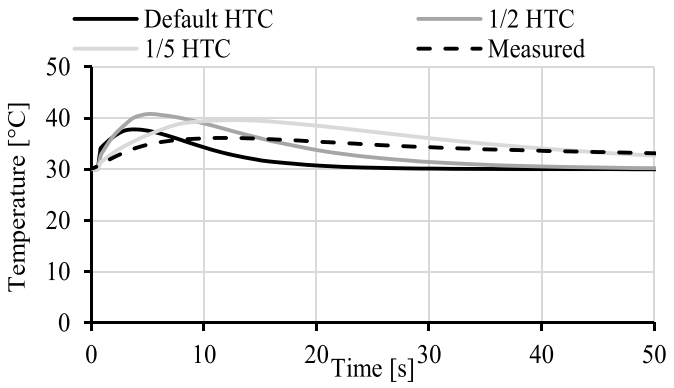

Fig. 15. Comparison of the temperatures at the location of the thermocouple.

Maximal strain was modelled with adequate accuracy while core shift analysis showed acceptable deviation from the measured curve in the holding and in the residual cooling phases. Table 6 shows the ε_{yy} strain results. The difference in the measured and the calculated strain in the residual cooling phase can be attributed to two factors. First is the limited modelling of the thermal expansion of the insert and the second is the assumption of core shift analysis that the nodal displacements of the insert remain constant after the product freezes.

The proper injection moulding simulation model can be set up by analysing a set of different quantities (temperatures, product thicknesses and operational strains) then comparing them to the measured results. Based on the analysis of temperature distribution, the most accurate model was the 1/5 HTC model. Since the heat transfer primarily depends on the pressure inside the cavity, and the temperature difference between the mould walls and the injected polymer, every analysed case separately requires the determination of the suitable HTC values.

4.2. Moldflow–ANSYS Workbench coupled simulation

Section 4.1. shows that core shift analysis can yield fairly accurate results in terms of operational deformations, mould insert temperature and product dimensional accuracy. However, some shortcomings of this method were also illustrated, including the limited modelling of the thermal expansion of the insert (in the holding and residual cooling phases) and the springback of the cooling product and the insert. In order to consider these effects properly, we used a coupled simulation, where the mould mesh, the pressure and temperature results of the injection moulding simulation were exported with the use of the "mpi2ans" macro in Moldflow. The mould mesh was imported to ANSYS Workbench Mechanical 2019 and the pressure was applied as a list of nodal force loads (in each time step) on the mesh of the insert. Analysis type was "Static structural". We applied the same time stepping as earlier in the Moldflow simulation. Insert temperature was considered a "Thermal Condition", which means that the entire insert has a uniform, time dependent temperature distribution. It is a proper assumption, since this aluminium grade has outstanding thermal conductivity (~147 W/(m·K)). The temperature–time curve, measured by the thermocouple, was used as an input for the simulation. Surfaces where the insert can come into contact with the mould housing had "Compression only supports" applied. These supports prevent deformations normal to the surface, towards the direction of the mould housing or the product. However, the insert can detach from these supports if it deforms in the opposite direction. Fig. 19 shows the applied boundary conditions and the input temperature–time curve.

Fig. 20 shows the calculated total deformation field of the insert (approximately at the maximal deformation). The cavity is deformed by

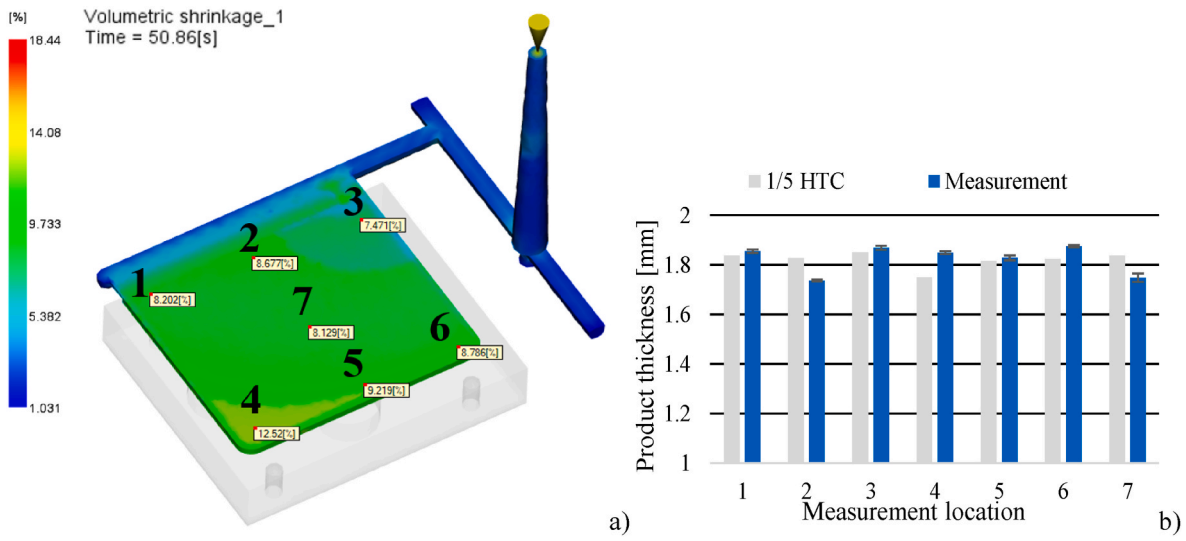

Fig. 16. The calculated volumetric shrinkage at 1/5 HTC a). The calculated product thickness and the comparison with the measured values b).

Table 5
Comparison of the calculated and measured product thicknesses with the use of the 1/5 heat transfer coefficients.

Location	1	2	3	4	5	6	7
1/5 HTC	1.836	1.826	1.851	1.75	1.816	1.824	1.837
Measured average	1.855	1.737	1.868	1.85	1.828	1.874	1.748
Deviation	−1.03 %	+5.16 %	−0.95 %	−5.40 %	−0.66 %	−2.67 %	+5.09 %

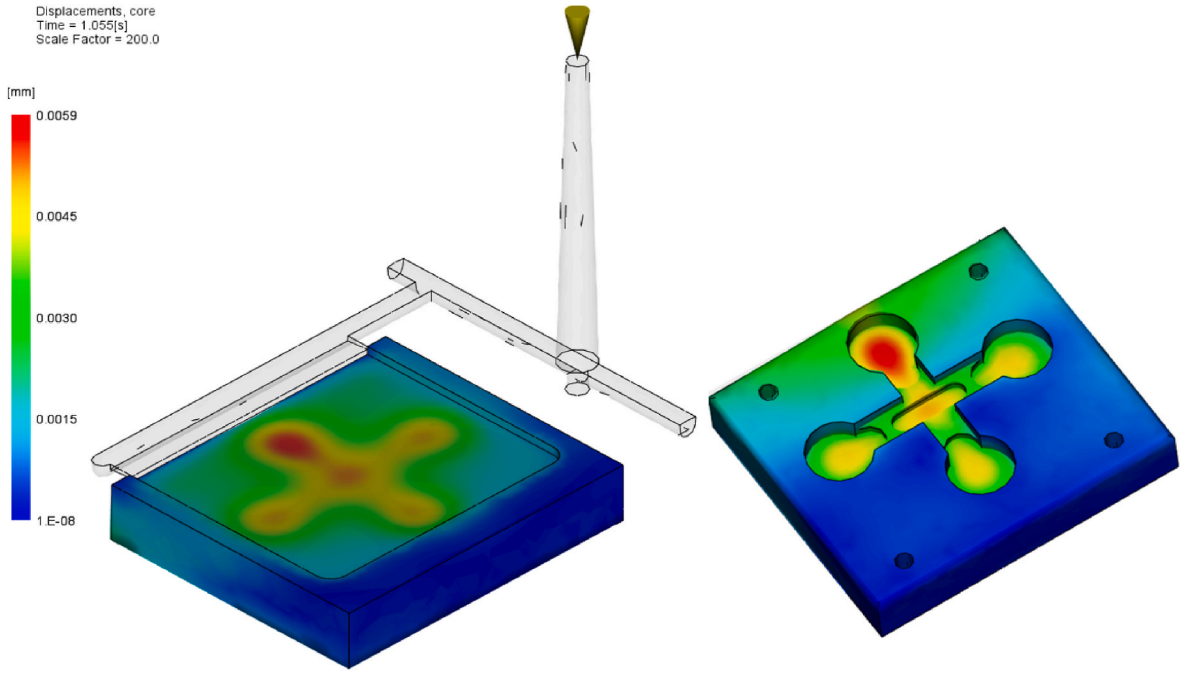

Fig. 17. The displacement field of core shift analysis results.

the applied pressure and the slots at the back also shrink due to thermal expansion. The ANSYS simulation considers the effect of thermal expansion much more accurately than core shift analysis.

The calculated normal strain ε_{yy} in the Y direction was compared to the measured strain. In ANSYS Workbench, the directional strains can be directly queried from the model, therefore no manual calculations are needed from the nodal displacements. The strains inside the two slots were queried at the location of the strain gauges (Fig. 13) and compared to the measured strains (Fig. 21). The coupled ANSYS–Moldflow simulation can significantly enhance the accuracy of the modelling of deformation. The simulated strain is close to the measured strain almost throughout the entire injection moulding cycle. Measured strains are necessarily heavily dependent on the imperfect contacts between the mould components (caused by the slight dimensional inaccuracies and manufacturing tolerances), while the mechanical simulation assumes perfect contacts at the boundary conditions. These effects cause some

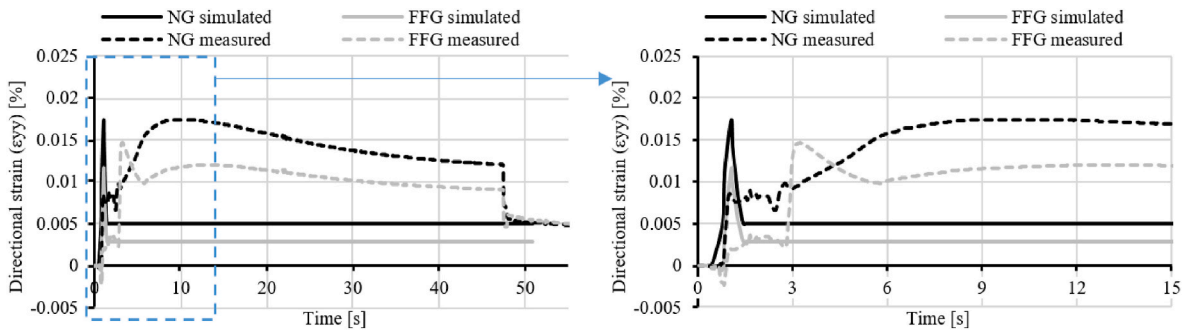

Fig. 18. Comparison of the measured strains (5 t clamping force) and the directional strains calculated from the core shift simulations 1/5 HTC c)).

Table 6
Comparison of the measured ε_{yy} strains and the strains calculated by core shift analysis.

Analysed quantity	1/5 HTC (Near the gate)	Measured (Near the gate)	1/5 HTC (Far from the gate)	Measured (Far from the gate)
Maximal ε_{yy} strain [%]	0.0173	0.0174	0.0114	0.0147
Deviation from the measured ε_{yy} strain [%]	−0.0001	–	−0.0033	–
Time of the maximal ε_{yy} strain [s]	1.05	9	1.05	3.2

slight deviations between the measurement and simulation but the accuracy of the calculation is clearly satisfactory.

If the deformational state of the mould components can be modelled with satisfactory accuracy, mould makers can optimise their designs to become more reliable. The size deviations of injection moulded products can also be estimated, which reduces the necessary injection mould trials. We proved that a combination of injection moulding simulation and finite element simulation, supported by the measurement results of a comprehensive state monitoring system could yield good results. There is good agreement between simulation and measurement if an adequate amount of strain, temperature and pressure measurement data is available.

Another important advantage of the coupled simulation approach is that it can consider more complex mould insert material models, not just linear elasticity (only available in Moldflow Insight's core shift

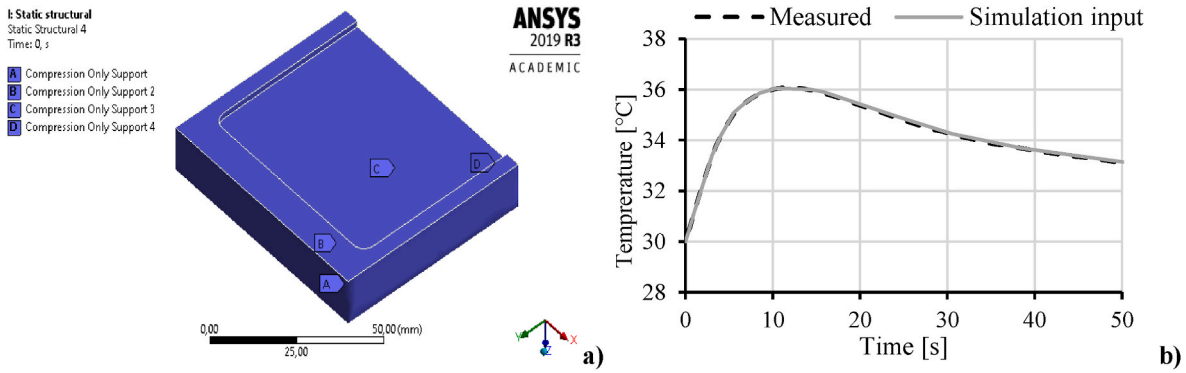

Fig. 19. ANSYS simulation model with the boundary conditions a) and the input temperature–time curve b).

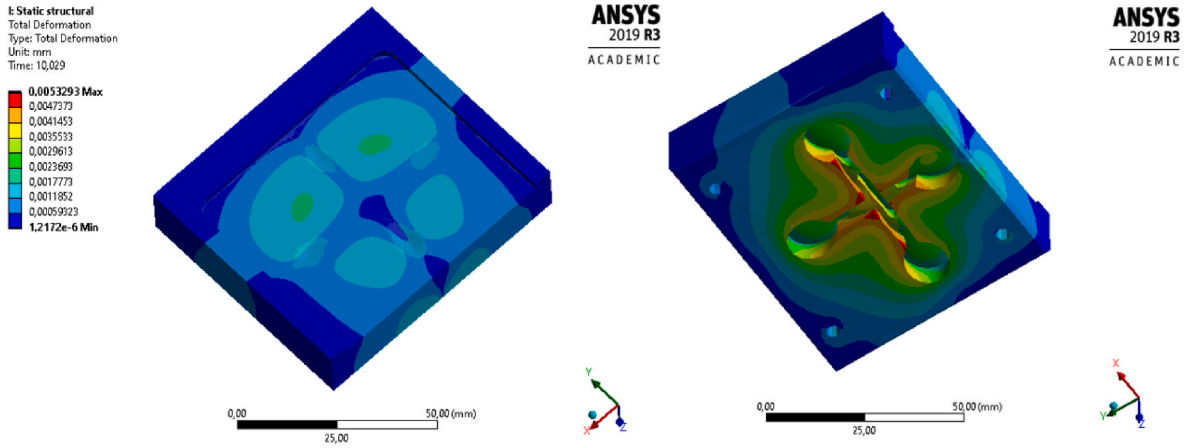

Fig. 20. Total deformation field of the ANSYS simulation model.

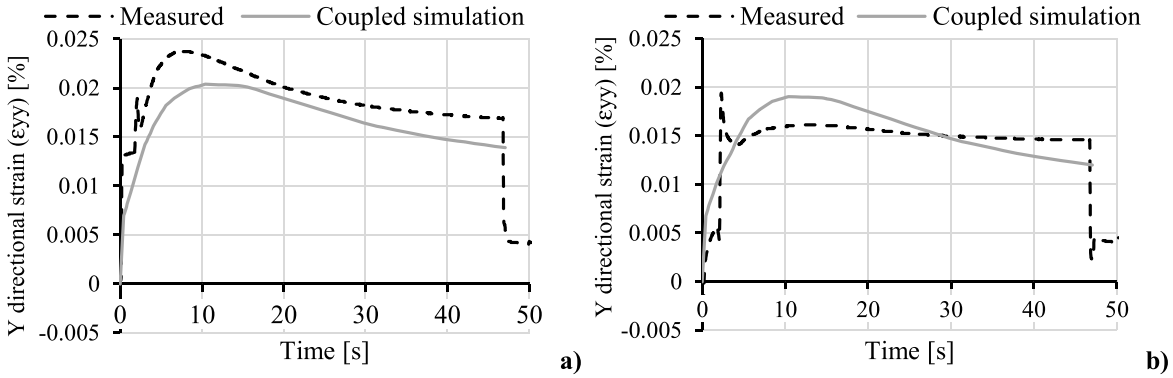

Fig. 21. Comparison of the calculated normal strains in the Y direction (using the coupled Moldflow–ANSYS simulation) and the measured strains near the gate a) and far from the gate b) (15 t clamping force).

analysis). The practical relevance of more complex material models become increasingly important as new, polymeric moulds and product inserts gain ground in the industry. A high-end finite element mechanical simulation software like ANSYS Workbench Mechanical also hosts viscoelastic material models that are suitable to model such polymeric moulds and inserts. The proper finite element modelling of mould inserts (especially polymeric inserts) is scarce, this area still has a large research potential.

5. Summary

We presented the combined effects of clamping force and holding pressure on the resulting operational strains and cavity pressures of an aluminium injection mould insert. Aluminium was selected because it is the traditional material of prototype mould making. With constant operational parameters, the increase in clamping force resulted in increasing cavity pressures. A greater clamping force resulted in more converging relative strain curves because partial mould opening did not occur. Correlational diagrams were produced between the integrals of the cavity pressure curves and the resulting product mass and thickness. If proper clamping can be achieved and mould opening does not occur, the cavity pressure integral can predict product mass and thickness with confidence (mostly $R^2 > 0.9$, assuming a linear relationship between the pressure integral and the product mass and thickness).

We also modelled the deformation of the insert in Moldflow Insight 2021 using its Core Shift module. The calculated operational strains, temperatures and product dimensions were compared with the measured data. We also presented a novel modelling method, where transient pressure fields (obtained from injection moulding simulation) and measured volumetric temperature data are used to model the deformation of the insert in a professional mechanical finite element simulation software (ANSYS Workbench Mechanical 2019). The results of the two simulations were compared with the measured strains. Core shift simulation can predict maximal deformations accurately but it largely neglects thermal expansion and the springback of the cooling product in the holding and residual cooling phases. Therefore, we created the coupled injection moulding–mechanical simulation model, and found good agreement between the calculated and the measured strains. Based on these findings, the deformation of the aluminium mould insert can be modelled with both core shift simulation and the coupled injection moulding–finite element mechanical simulation. The latter simulation is more accurate when modelling the entire IM cycle, not just maximal deformation.

The coupled simulation method outlined in this paper can be especially useful if the mould insert material cannot be modelled adequately by simple linear elasticity with constant material parameters, for example, in the case of polymeric mould inserts, where creep and a temperature-dependent modulus of elasticity has to be considered. This study paves the way for such coupled and more elaborate simulations.

Funding

Project no. TKP-6-6/PALY-2021 has been implemented with the support provided by the Ministry of Culture and Innovation of Hungary from the National Research, Development and Innovation Fund, financed under the TKP2021-NVA funding scheme. Project no. RRF-2.3.1-21-2022-00009, titled National Laboratory for Renewable Energy has been implemented with the support provided by the Recovery and Resilience Facility of the European Union within the framework of Programme Széchenyi Plan Plus. Supported by the ÚNKP-22-3-II-BME-105 New National Excellence Program of the Ministry for Culture and Innovation from the source of the National Research, Development and Innovation Fund. This work was supported by the National Research, Development and Innovation Office, Hungary (OTKA FK134336).

Declaration of competing interest

The authors declare that they have no known competing financial interests or personal relationships that could have appeared to influence the work reported in this paper.

Data availability

Data will be made available on request.

Acknowledgements

The authors wish to thank ARBURG HUNGÁRIA KFT. for the ARBURG Allrounder injection moulding machine, and TOOL-TEMP HUNGÁRIA KFT., LENZKES GMBH and PIOVAN HUNGARY KFT. for the accessories.

References

[1] C. Macedo, A.M. Brito, L. Faria, C.L. Simões, J. Laranjeira, R. Simoes, The potential of RHCM technology in injection molding using a simple convention heating and cooling system, Results Eng. 19 (2023), 101349, https://doi.org/10.1016/j.rineng.2023.101349.

[2] C. Berges, J. Hidalgo, R. Andújar, R. Campana, G. Herranz, Prospects of producing solid oxide fuels interconnectors processed by metal injection moulding, Results Eng. 11 (2021), 100268, https://doi.org/10.1016/j.rineng.2021.100268.

[3] J.A. Naranjo, C. Berges, R. Campana, G. Herranz, Rheological and mechanical assessment for formulating hybrid feedstock to be used in MIM & FFF, Results Eng. 19 (2023), 101258, https://doi.org/10.1016/j.rineng.2023.101258.

[4] C.-C. Kuo, Z.-F. Jiang, X.-Y. Yang, S.-X. Chu, J.-Q. Wu, Characterization of a direct metal printed injection mold with different conformal cooling channels, Int. J. Adv. Des. Manuf. Technol. 107 (2020) 1223–1238, https://doi.org/10.1007/s00170-020-05114-2.

[5] S.J. Park, J.H. Lee, J. Yang, W. Heogh, D. Kang, S.M. Yeon, S.H. Kim, S. Hong, Y. Son, J. Park, Lightweight injection mold using additively manufactured Ti-6Al-

4V lattice structures, J. Manuf. Process. 79 (2022) 759–766, https://doi.org/10.1016/j.jmapro.2022.05.022.
[6] H.-S. Park, X.-P. Dang, Development of a smart plastic injection mold with conformal cooling channels, Procedia Manuf. 10 (2017) 48–59, https://doi.org/10.1016/j.promfg.2017.07.020.
[7] D. Török, B. Zink, T. Ageyeva, I. Hatos, M. Zobač, I. Fekete, R. Boros, H. Hargitai, J. G. Kovács, Laser powder bed fusion and casting for an advanced hybrid prototype mold, J. Manuf. Process. 81 (2022) 748–758, https://doi.org/10.1016/j.jmapro.2022.07.034.
[8] F. Lupone, E. Padovano, M. Pietroluongo, S. Giudice, O. Ostrovskaya, C. Badini, Optimization of selective laser sintering process conditions using stable sintering region approach Express, Polymer Letters 15 (2) (2021) 177–192, https://doi.org/10.3144/expresspolymlett.2021.16.
[9] R. Alkentar, T. Mankovits, A study on the shape and dimensional accuracy of additively manufactured titanium lattice structures for orthopedic purposes, Period. Polytech. - Mech. Eng. 66 (4) (2022) 336–343, https://doi.org/10.3311/PPme.20382.
[10] R. Mahshid, H.N. Hansen, K.L. Højbjerre, Strength analysis and modeling of cellular lattice structures manufactured using selective laser melting for tooling applications, Mater. Des. 104 (2016) 276–283, https://doi.org/10.1016/j.matdes.2016.05.020.
[11] M. Narvan, A. Ghasemi, E. Fereiduni, S. Kendrish, M. Elbestawi, Part deflection and residual stresses in laser powder bed fusion of H13 tool steel, Mater. Des. 204 (2021), 109659, https://doi.org/10.1016/j.matdes.2021.109659.
[12] B. Zink, N.K. Kovács, J.G. Kovács, Thermal analysis based method development for novel rapid tooling applications, Int. Commun. Heat Mass Tran. 108 (2019), 104297, https://doi.org/10.1016/j.icheatmasstransfer.2019.104297.
[13] G.A. Mendible, J.A. Rulander, S.P. Johnston, Comparative study of rapid and conventional tooling for plastics injection molding, Rapid Prototyp. J. 23 (2) (2017) 344–352, https://doi.org/10.1108/RPJ-01-2016-0013.
[14] I. Ilyas, C. Taylor, K. Dalgarno, J. Gosden, Design and manufacture of injection mould tool inserts produced using indirect SLS and machining processes, Rapid Prototyp. J. 16 (6) (2010) 429–440, https://doi.org/10.1108/13552541011083353.
[15] A. Davoudinejad, M.R. Khosravani, D.B. Pedersen, G. Tosello, Influence of thermal ageing on the fracture and lifetime of additively manufactured mold inserts, Eng. Fail. Anal. 115 (2020), 104694, https://doi.org/10.1016/j.engfailanal.2020.104694.
[16] T. Ageyeva, Sz Horváth, J.G. Kovács, In-Mold sensors for injection molding: on the way to industry 4.0, Sensors 19 (2019), https://doi.org/10.3390/s19163551, 3551/1-3551/21.
[17] R.D. Párizs, D. Török, T. Ageyeva, J.G. Kovács, Machine learning in injection molding: an industry 4.0 method of quality prediction, Sensors 22 (2022), https://doi.org/10.3390/s22072704, 2704/1-2704/16.
[18] A.S. Struchtrup, D. Kvaktun, R. Schiffers, A holistic approach to part quality prediction in injection molding based on machine learning, in: Advances in Polymer Processing 2020, Springer, Berlin/Heidelberg, Germany, 2020, pp. 137–149, https://doi.org/10.1007/978-3-662-60809-8_12.
[19] K.-C. Ke, M.-S. Huang, Quality classification of injection-molded components by using quality indices, grading, and machine learning, Polymers 13 (3) (2021) 353, https://doi.org/10.3390/polym13030353.
[20] M. Vukovic, S. Stemmler, K. Hornberg, D. Abel, C. Hopmann, Adaptive model-based predictive control for cross-phase cavity pressure control in injection molding, J. Manuf. Process. 77 (2022) 730–742, https://doi.org/10.1016/j.jmapro.2022.02.030.
[21] X. Zhou, Y. Zhang, T. Mao, H. Zhou, Monitoring and dynamic control of quality stability for injection molding process, J. Mater. Process. Technol. 249 (2017) 358–366, https://doi.org/10.1016/j.jmatprotec.2017.05.038.
[22] Q. Wang, X. Zhao, J. Zhang, P. Zhang, X. Wang, C. Yang, J. Wang, Z. Wu, Research on quality characterization method of micro-injection products based on cavity pressure, Polymers 13 (16) (2021) 2755, https://doi.org/10.3390/polym13162755.
[23] M. Kurt, O. Saban Kamber, Y. Kaynak, G. Atakok, O. Girit, Experimental investigation of plastic injection molding: assessment of the effects of cavity pressure and mold temperature on the quality of the final products, Mater. Des. 30 (2009) 3217–3224, https://doi.org/10.1016/j.matdes.2009.01.004.
[24] K.-M. Tsai, H.-J. Luo, Comparison of injection molding process windows for plastic lens established by artificial neural network and response surface methodology, Int. J. Adv. Manuf. Technol. 77 (2015) 1599–1611, https://doi.org/10.1007/s00170-014-6366-6.
[25] J.-Y. Chen, J.-X. Zhuang, M.-S. Huang, Enhancing the quality stability of injection molded parts by adjusting V/P switchover point and holding pressure, Polymer 213 (2021), 123332, https://doi.org/10.1016/j.polymer.2020.123332.
[26] C.-W. Su, W.-J. Su, F.-J. Cheng, G.-Y. Liou, S.-J. Hwang, H.-S. Peng, H.-Y. Chu, Optimization process parameters and adaptive quality monitoring injection molding process for materials with different viscosity, Polym. Test. 109 (2022), 107526, https://doi.org/10.1016/j.polymertesting.2022.107526.
[27] Sz. Krizsma, N.K. Kovács, J.G. Kovács, A. Suplicz, In-situ monitoring of deformation in rapid prototyped injection molds, Addit. Manuf. 42 (2021), https://doi.org/10.1016/j.addma.2021.102001, 102001/1-102001/8.
[28] Sz. Krizsma, A. Suplicz, Comprehensive in-mould state monitoring of Material Jetting additively manufactured and machined aluminium injection moulds, J. Manuf. Process. 84 (2022) 1298–1309, https://doi.org/10.1016/j.jmapro.2022.10.070.
[29] R. Mahshid, Y. Zhang, H.N. Hansen, A.H. Slocum, Effect of mold compliance on dimensional variations of precision molded components in multi-cavity injection molding, J. Manuf. Process. 67 (2021) 12–22, https://doi.org/10.1016/j.jmapro.2021.04.048.
[30] Y. Zhao, P. Zhao, J. Zhang, J. Huang, N. Xia, J. Fu, On-line measurement of clamping force for injection molding machine using ultrasonic technology, Ultrasonics 91 (2019) 170–179, https://doi.org/10.1016/j.ultras.2018.08.013.
[31] M.-S. Huang, C.-Y. Lin, A novel clamping force searching method based on sensing tie-bar elongation for injection molding, Int. J. Heat Mass Tran. 109 (2017) 223–230, https://doi.org/10.1016/j.ijheatmasstransfer.2017.02.004.
[32] J.T. Jung, L. Bong Kee, Fluid-structure interaction model to predict deformation of mold cores in injection molding filling stage, J. Mech. Sci. Technol. 32 (2) (2018) 817–822, https://doi.org/10.1007/s12206-018-0132-2.
[33] B. Zink, J.G. Kovács, Pressure-dependent heat transfer coefficient measurement for thermoplastic melts, Polym. Eng. Sci. 62 (2022) 1137–1146, https://doi.org/10.1002/pen.25912.
[34] A. Bakharev, Z. Fan, F. Costa, Prediction of Core Shift Effects Using Mold Filling Simulation, ANTEC, 2007.